Some Comparisons of Impact Craters on Mercury and the Moon

DONALD E. GAULT,[1] JOHN E. GUEST,[2] JOHN B. MURRAY,[2] DANIEL DZURISIN,[3] AND MICHAEL C. MALIN[3]

Although the general morphologies of fresh mercurian and lunar craters are remarkably similar, comparisons of ejecta deposits, interior structures, and changes in morphology with size reveal important differences between the two populations of craters. The differences are attributable to the different gravity fields in which the craters were formed and have significant implications for the interpretation of cratering processes and their effects on all planetary bodies.

INTRODUCTION

With additional evidence from the Mariner 10 photography of Mercury [*Murray et al.*, 1974*a*, *b*], as well as the recent radar observations of Venus [*Rumsey et al.*, 1974], it is now firmly established that impact cratering has been a geologic process of primary significance in the evolution of all the terrestrial planets (and undoubtedly all planetary objects). The heavily cratered surfaces of Mercury, the moon, and Mars document the earliest stages of their planetary histories, and it is clear that a thorough understanding of cratering processes and formation is essential for gaining further insight into the early history and subsequent development of all the terrestrial planets. Although the early cratering record of earth has been erased irrevocably and lost by the action of other more active geologic processes, the recent and relatively young terrestrial impact structures have been important for an understanding and interpretation of lunar (and martian) craters and cratering processes [e.g., *Shoemaker*, 1962; *Baldwin*, 1963]. Conversely, studies of lunar (martian) craters offer a means for comparisons with terrestrial craters and cratering phenomena in general [e.g., *Hartmann*, 1972]. However, such empirical approaches to the study and evaluation of cratering on different planetary bodies have limitations; impact cratering is a complex physical process that is dependent on many parameters, and unless the functional dependences are known or recognized and relationships are established, cratering criteria developed from craters formed in one planetary environment may not be applicable to similar processes and effects in a different environment. Moreover, erosion of martian and terrestrial craters by agents foreign to the moon has been so severe that it seems questionable whether valid comparisons can be made between craters on the three bodies; that is, the lack of fresh, sharp impact structures on earth and Mars precludes, or at least obscures, evaluation of any differences in the cratering processes and crater forms arising from differences in their planetary environment.

In marked contrast, however, the mercurian craters from the Mariner 10 photography provide comparisons with lunar craters under almost ideal 'experimental' conditions. With no appreciable atmosphere having enveloped either body since the very earliest stages of their history nor any fluvial action [*Murray et al.*, 1974*b*, 1975], only one prime cratering variable has been different between the two crater populations, gravitational acceleration. Differences in physical properties, impact velocities, possibly thermal history, etc., may have contributed some different effects, but the influence of these variables should be of second-order importance, at best, in comparison with the gravitational effects. There are, for example, compelling arguments [*Murray et al.*, 1974*b*, 1975] that the fresh mercurian craters, which are of interest for comparative purposes, have been formed in silicates at least grossly similar to those of the moon and, hence, would provide similar physical properties and response during cratering at the scale of impact events of interest (diameters greater than a few kilometers). Similarly, although impact velocities in excess of 130 km/s are possible for Mercury, the average mercurian impact velocities for comparative purposes are probably in the range of 25–30 km/s, within a factor of 2 greater than typical lunar values [*Wetherill*, 1975]. Higher impact velocities will provide increases in the vapor and melt products of the mercurian events, but the effects on the style of cratering and final crater morphology should be negligible.

It is the purpose of this paper therefore to present first results of some comparisons of the morphology of mercurian and lunar craters in order to explore differences in cratering style and final landforms caused by what are probably predominately differences in gravitational forces and induced stresses. In what follows, the morphology and examples of mercurian craters which were studied in detail are followed by a brief consideration of scaling (crater size) relationships, comparisons of quantitative measurements of ejecta deposits surrounding craters, comparisons of statistics of interior crater morphological elements, and discussion with implications for planetary cratering in general.

MORPHOLOGY OF MERCURIAN CRATERS

The morphology of mercurian craters is grossly similar to that of lunar craters; i.e., the morphologic elements (rim facies, satellitic craters, inner terraced walls, central peak(s) and inner mountain rings) that characterize lunar impact craters are all associated with craters on Mercury. As with the moon, it can be demonstrated that with increasing age the morphology of craters becomes less sharp until most of the crater elements are barely recognizable and the crater is degraded to a low rim superposed with large numbers of impact craters. The dominant denudation process is apparently, as on the moon, the same process which produced the original crater, erosion and sedimentation by meteoritic bombardment.

The freshest craters away from the terminator have well-developed and extensive bright ray systems, many of them extending for hundreds of kilometers and a few extending in excess of 1000 km (Figure 1). Some craters are also surrounded by dark halos resembling those associated with such lunar craters as Tycho and Aristarchus; these are best seen near the limb under conditions approaching zero phase lighting. Other

[1] Ames Research Center, NASA, Moffett Field, California 94035.
[2] University of London Observatory, Mill Hill Park, London, England.
[3] Division of Geological and Planetary Sciences, California Institute of Technology, Pasadena, California 91109.

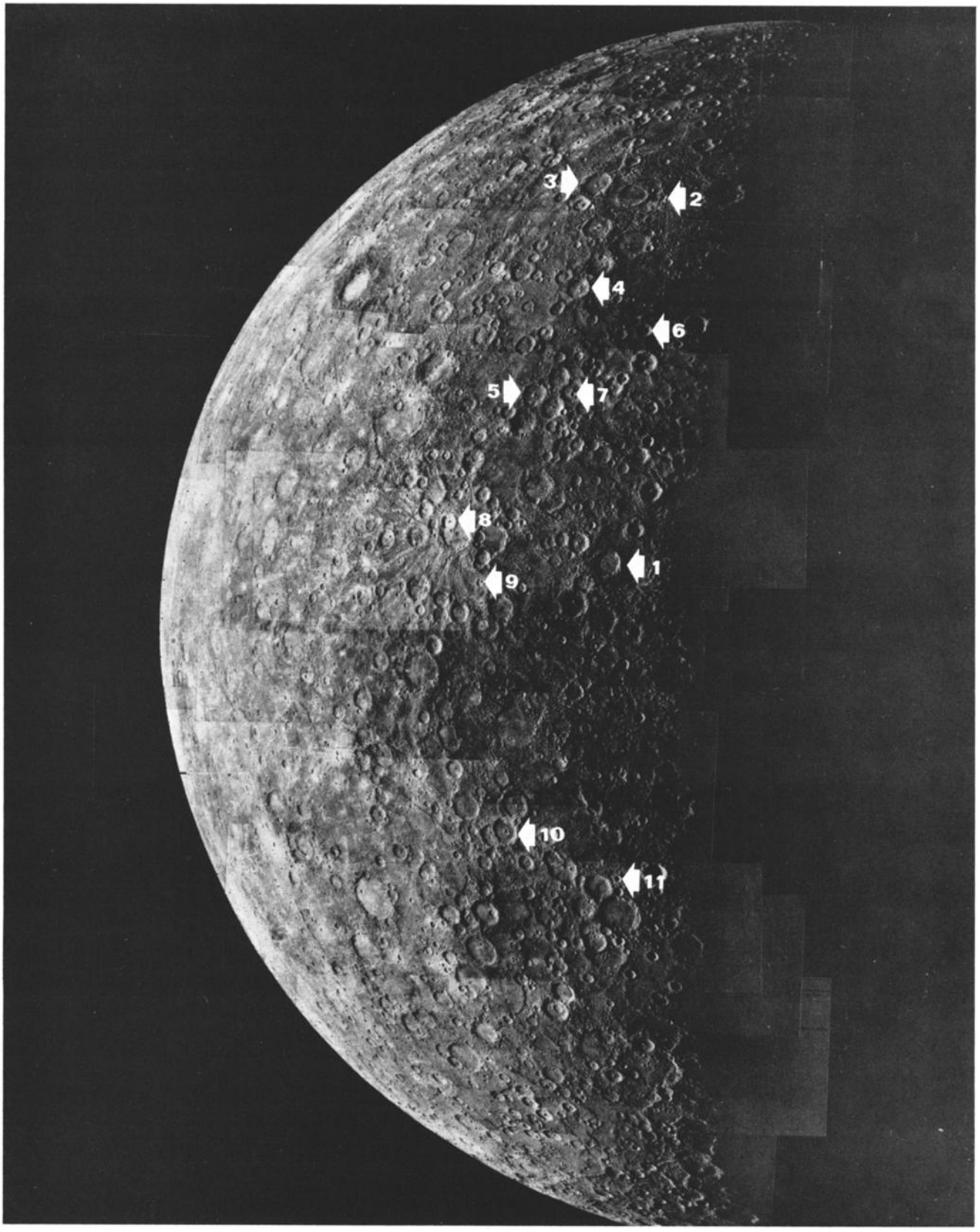

Fig. 1*a*. Preencounter view of planet with evening terminator.

Fig. 1. Photomosaics of Mercury showing location of craters selected for detailed study of their morphology and ejecta deposits. Coordinates and diameters of craters are listed in Table 1.

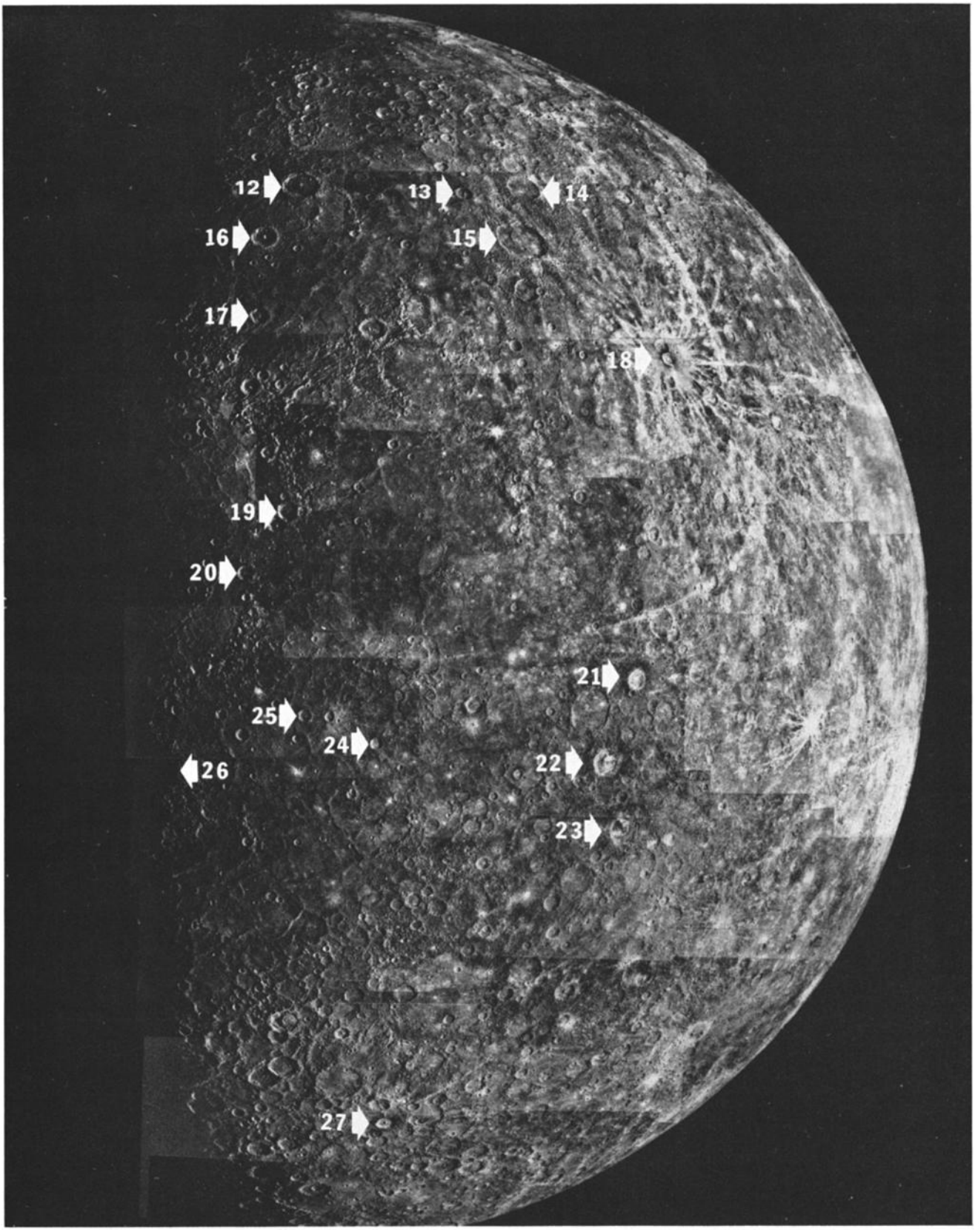

Fig. 1*b*. Postencounter view of planet with morning terminator.

fresh craters appear to have lost their ray systems and dark halos, but they remain fresh in all other respects.

The morphology of the outer rim units of the mercurian craters distinguishes them from their lunar counterparts. At earth-based resolution of the moon, which is comparable to the available resolution for most of the mercurian craters, the rims of lunar craters appear to consist of an inner hummocky facies that grades out into a radially ridged facies [e.g., *Guest,* 1973]; these facies make up what is termed the continuous ejecta blanket and grade outwards into a zone of satellitic craters forming crater clusters and chains, interpreted as secondary impact craters and discontinuous ejecta deposits. On the mercurian craters the hummocky rim facies is well-developed but grades out over a relatively short distance through the radially ridged facies into a zone characterized by satellitic craters (Figure 2). The areal density of craters in this outer region is very high and gives the impression that the surface is close to saturation [*Gault,* 1970]. For craters with diameters greater than approximately 150 km, crater chains are extremely well developed to give long linear grooves (predominately radial to the crater) with crater form, scalloped rims; in some cases the grooves extend across the rim facies near the crater rim crest (Figure 3), a phenomenon rarely seen on lunar craters. High-resolution pictures of the mercurian secondary crater fields reveal that the craters are less circular than normal primary impact craters and that the craters are often elongate with their long axis radial to the primary crater. The herringbone pattern and V-shaped features associated with lunar secondary craters [*Guest and Murray,* 1971; *Oberbeck and Morrison,* 1973] are not generally found on the mercurian craters probably because of resolution limits, but on one of the highest resolution pictures, such features appear to be present (Figure 4), suggesting that this phenomenon is not unique to the moon.

The interior structure of mercurian craters is dependent on size, much in the same manner as has been noted before for lunar craters [*Stuart-Alexander and Howard,* 1970; *Hartmann and Wood,* 1971]. The smaller craters are predominately bowl-shaped cavities, but with increasing size some central peaks are evident, and slump features develop on the walls and may fill most of the bottom of the crater (Figure 5). For still larger craters the inner slumping forms well-developed terraces that do not extend across the entire crater floor; the floors tend to be hilly, but nevertheless, flatter and rising from them are central peaks or clusters of peaks (Figures 6 and 7). The largest craters, which would be called basins in lunar terminology, are characterized by a ringed complex of peaks or a complete mountainous ring concentric with the crater rim (Figure 8).

Fig. 2. Crater 16 (98-km diameter) illustrates the narrow hummocky rim facies, radial ridges, and surrounding extensive field of secondary craters. The well-developed interior terraces and central peaks are typical for mercurian craters in this size range. Note that the smaller craters in the foreground (~25-km diameter) also are terraced. Flight Data Subsystem (FDS) frame 80.

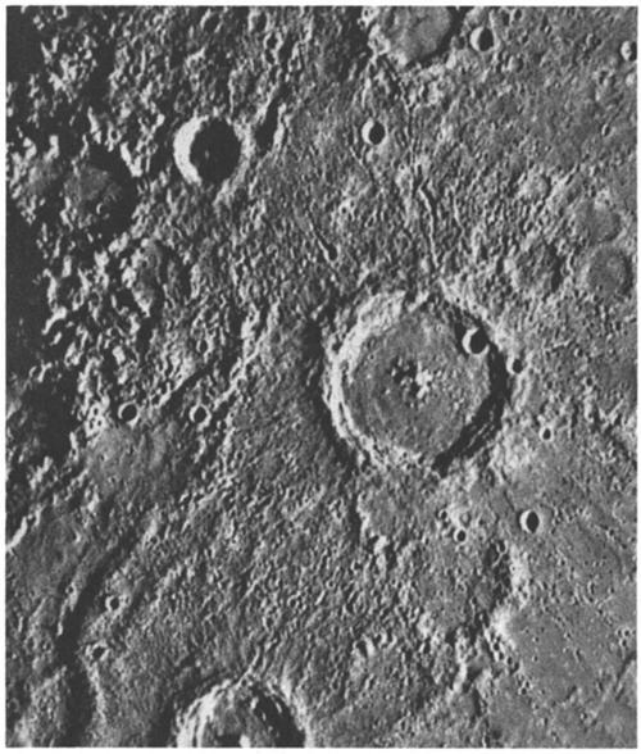

Fig. 3. Orthographic projection of FDS frame 166 showing the 140-km diameter crater 12 and its surrounding zone of secondary craters. The narrow width of the rim facies, the prominent subradial secondary crater chains, and grooves are representative for the larger mercurian craters.

The sizes of mercurian craters in this progression of interior structures are systematically less than for lunar craters; quantitative values will be presented later.

Crater Scaling

There is firm theoretical and experimental evidence that gravitational acceleration is an important parameter affecting the size of craters formed by either explosives or impact [*Viktorov and Stepenov,* 1960; *Chabai,* 1965; *Johnson et al.,* 1969; D. E. Gault and J. A. Wedekind, manuscript in preparation, 1975]. Thus an important difference that must be anticipated to exist between mercurian and lunar craters, for which the Mariner 10 imagery cannot provide a basis for comparisons, consists of the effects of gravity on the dimensions of their respective excavation craters. Here, by definition, excavation crater is taken to mean the crater attained as the direct result of processes related to stress (shock) waves which set material in motion to form the crater, in contrast to the final crater, which is the excavation crater modified by postcratering processes unrelated to the passage of stress waves. Because expected differences in the excavation craters on the two bodies are significant to subsequent discussions, a brief qualitative discussion of crater scaling criteria is given in the following paragraphs. For a more rigorous treatment of variables and problems of crater scaling (although the discussion is concerned specifically with craters formed by explosives), the reader is referred to *Chabai* [1965].

A simple approach to demonstrate the variations and applicable ranges of various scaling relationships is to consider the partition of energy for impact events; that is, we will consider how much and in what manner energy is expended during the formation of an excavation crater as a means of establishing a scaling relationship. Starting from the reservoir of kinetic energy KE represented by the motion of the impacting body relative to the surface of the planet, energy is expended for five main processes: heating, E_h; comminution, E_c; plastic and viscous deformations, E_{pv}; removal (ejection) of material from the crater, E_e; and seismic waves, E_s [see *Gault and Heitowit,* 1963; *Braslau,* 1970]. Although the shock compressions produced by impact are adiabatic processes, the associated increases in internal energy of the compressed masses are not accomplished isentropically (entropy constant), and internal energy is trapped irreversibly as heat after release of stresses to ambient conditions. This energy is manifested in melting and/or vaporization of both the impacting and the impacted material. The fraction of KE converted to heat is a function of the materials and the impact velocity V_i and can be expressed here as

$$E_h = k_1 f(V_i) \tag{1}$$

with k_1 a constant and $f(V_i)$ a function of impact velocity. It is worth noting that E_h represents a fraction of the KE that is lost to the cratering process because it does not contribute either directly or indirectly to removing material from the site of the impact during formation of the crater.

Comminution energy, the creation of free surfaces, is directly proportional to the volume of material crushed and broken up during the cratering event and is a function of the size distribution of the comminuted mass. Taking the volume of the crater proportional to the cube of its diameter D (i.e., the shape of the excavation crater is independent of size; see section on depth-diameter relationships), then it can be shown that the comminution energy can be written as

$$E_c = k_2 D^{3-\alpha\delta} \tag{2}$$

with k_2 a constant and where α and δ are positive valued terms used to describe the size distribution of the crushed material of the impact event. Similarly, the energy expended for plastic and/or viscous deformation as the embryonic crater develops to its final excavation size will be proportional also to the volume of the crater. By introducing another constant k_3 we arrive at

$$E_{pv} = k_3 D^3 \tag{3}$$

In contrast, the minimum energy necessary to remove (eject) the excavated material from the crater is proportional to the product of the crater volume, some average height the volume must be raised to deposit the ejecta around the crater, and the gravitational acceleration. Because the height can be taken proportional to the diameter, the minimum ejection energy becomes

$$E_e = k_4 g D^4 \tag{4}$$

with a fourth constant k_4 and the gravitational acceleration g. Finally, the shock waves produced by the impact attenuate with increasing distance from the point of impact and ultimately decay into a complex pattern of seismic waves containing a fraction of the original KE. The functional dependence is unknown, but for present purposes it can be written as

$$E_s = k_5 KE \tag{5}$$

Although this seismic energy is a very small fraction of KE ($k_5 \sim 10^{-4}$ to 10^{-5}), a Caloris event on Mercury or an Imbrium event on the moon (10^{34} ergs?) could produce a seismic wave

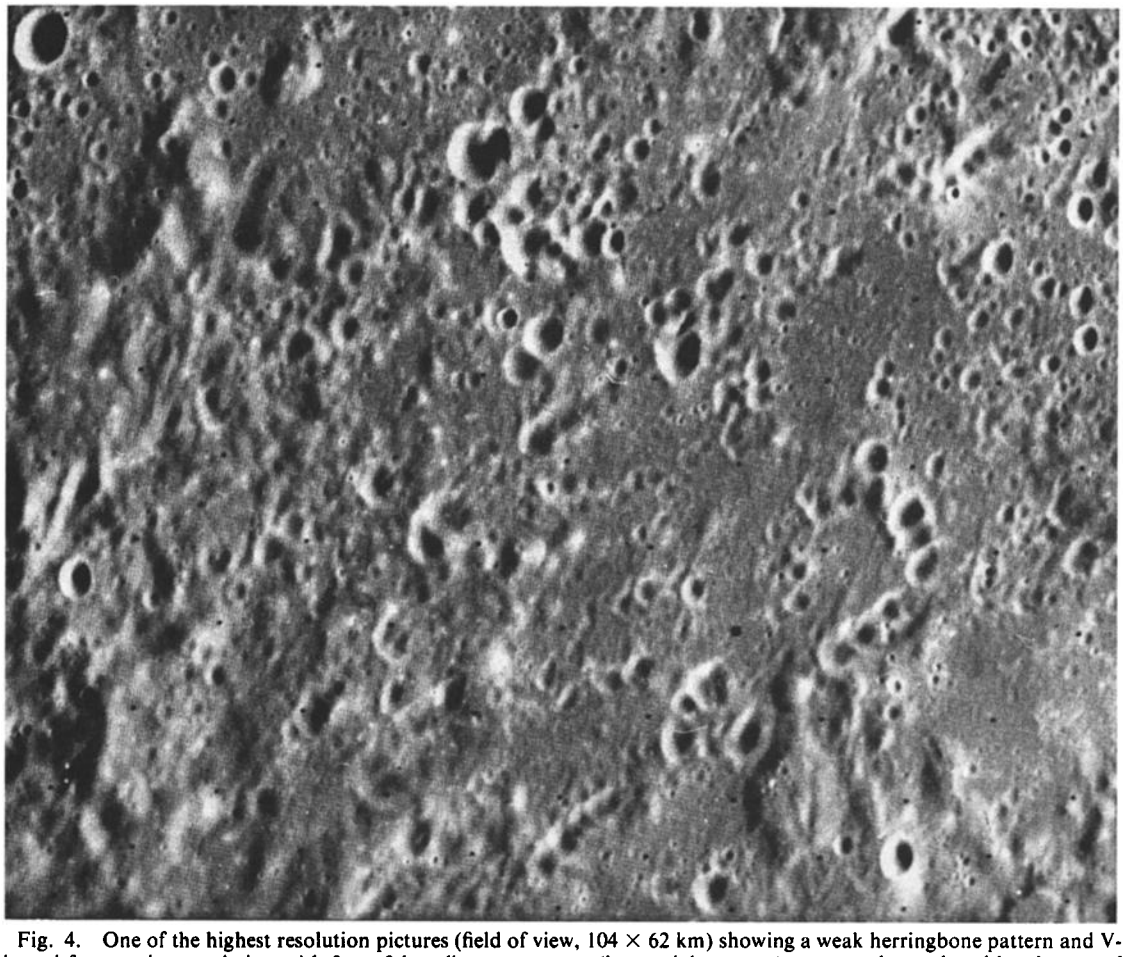

Fig. 4. One of the highest resolution pictures (field of view, 104 × 62 km) showing a weak herringbone pattern and V-shaped features in association with 2- to 3-km diameter craters (lower right corner), apparently produced by clusters of secondary ejecta from an unknown source ot the southwest (north up). FDS frame 51.

train orders of magnitude greater than the intensity of any known terrestrial earthquakes. Some speculations on the effects of seismic effects of such magnitudes are discussed by *Schultz and Gault* [1975], in particular the possible relation to the hilly and lineated terrain described by *Trask and Guest* [1975] that is antipodal to the Caloris basin.

Taking the sum of the five energy expenditures and equating them to the *KE* results in

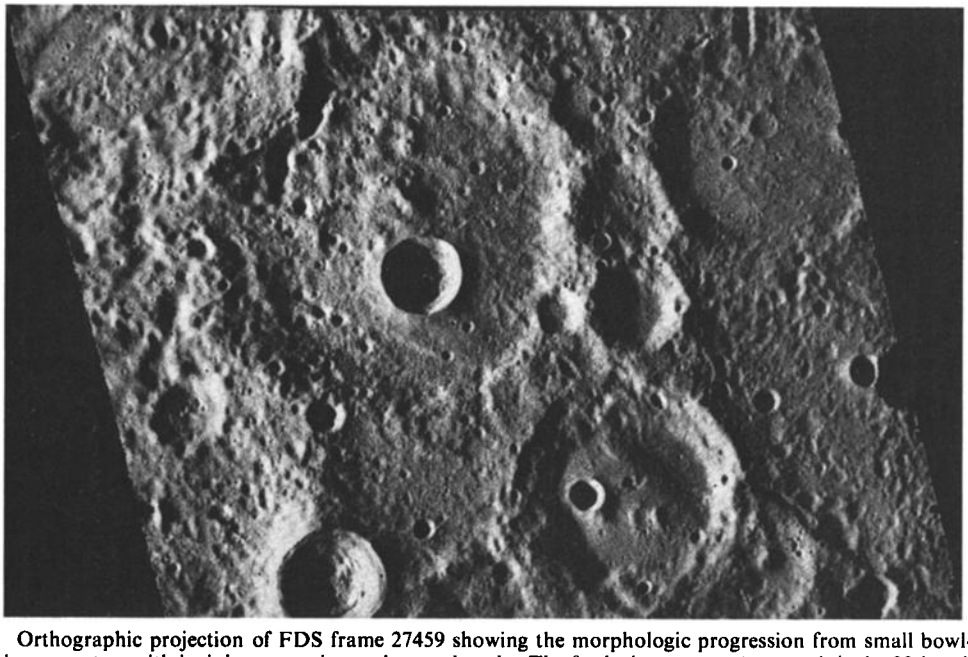

Fig. 5. Orthographic projection of FDS frame 27459 showing the morphologic progression from small bowl-shaped craters to larger craters with incipient terracing and central peaks. The fresh sharp crater (centered) is the 20-km diameter crater 7 with Mercury's surface longitude reference crater Hun Kal [*Davies and Batson*, 1975] on its southern flank.

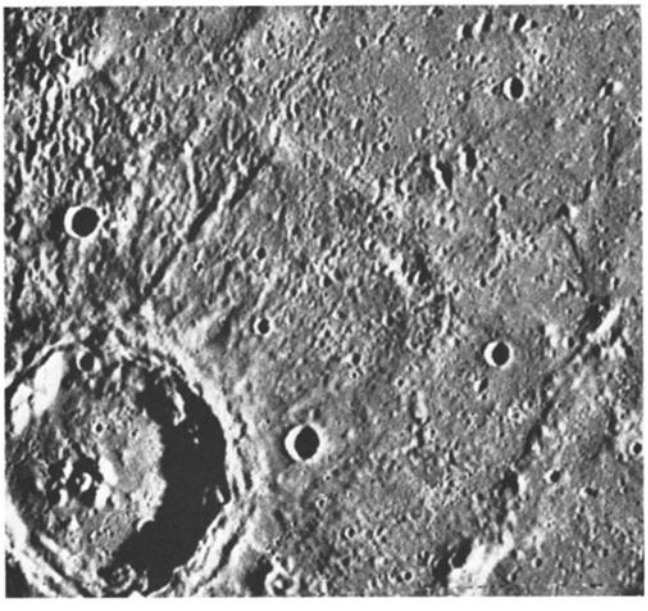

Fig. 6. Crater 17 (74-km diameter) just north of the Caloris Planitia displays interior terracing and central peaks rising up from a hilly floor. The continuous ejecta deposits and secondary crater field are well-defined. Orthographic projection, FDS frame 79.

$$KE = k_1 f(V_i) + k_2 D^{3-\alpha\delta} + k_3 D^3 + k_4 g D^4 + k_5 KE$$

If the KE is held constant as the impact velocity is increased, the fraction of KE converted to heat remains relatively constant (approximately 30–35% for silicate materials of interest) for velocities in excess of about 15 km/s (D. E. Gault, unpublished results, 1969). For this reason it is convenient to collect terms involving just KE,

$$F(KE) = KE - k_1 f(V_i) - k_5 KE$$

and rewrite the energy balance as

$$F(KE) \approx k_2 D^{3-\alpha\delta} + k_3 D^3 + k_4 g D^4$$

For craters in rock, k_2 will have a value of the order of 10^9 [see *Gault*, 1973], while k_4 will be less than 10^4 [*Gault and Heitowit*, 1963] but greater than 10^{-1} considering the minimum energy necessary to excavate a crater; on the basis of explosive cratering data, $k_3 \approx 10^7$. Thus $k_2 >> k_3 >> k_4$, so that for small cratering events on planetary bodies involving modest amounts of KE the two terms on the right become insignificant, and the diameter D is related to KE by

$$D \propto F(KE)^{1/(3-\alpha\delta)} \tag{6}$$

while for very large impacts the terms involving D^3 become insignificant and

$$D \propto g^{-1/4} F(KE)^{1/4} \tag{7}$$

with a transitional range between the two extremes of

$$D \propto F(KE)^{1/3} \tag{8}$$

The last equation is the same as the well-known cube root scaling relationship of *Lampson* [1946], and (7) expresses a fourth root dependence, the so-called gravity scaling relationship [*Chabai*, 1965]. The precise range of diameters (i.e., KE) over which each equation should be applicable is poorly defined,

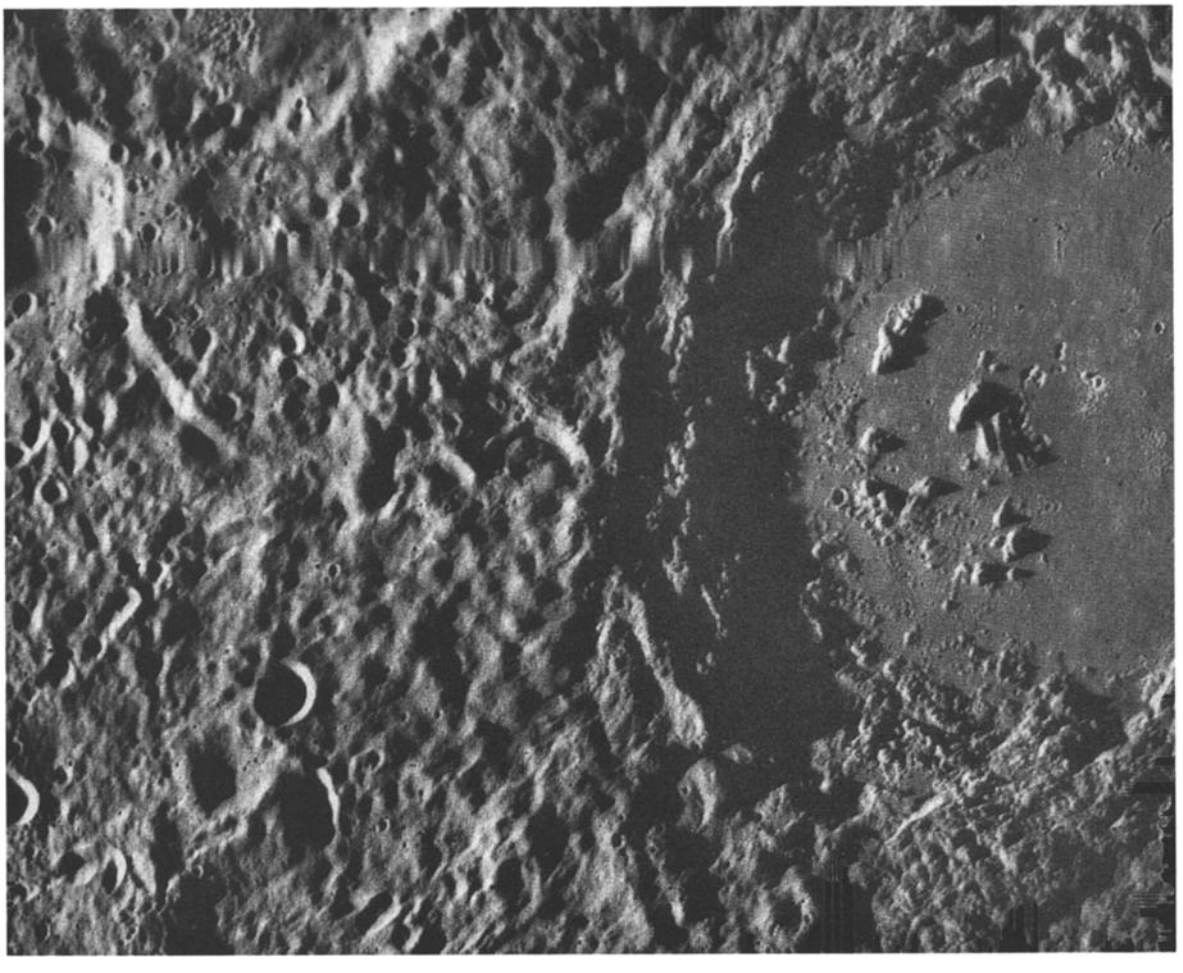

Fig. 7. Detailed view of a cluster of central peaks on the flat floor of crater 1 (120-km diameter). FDS frame 27461.

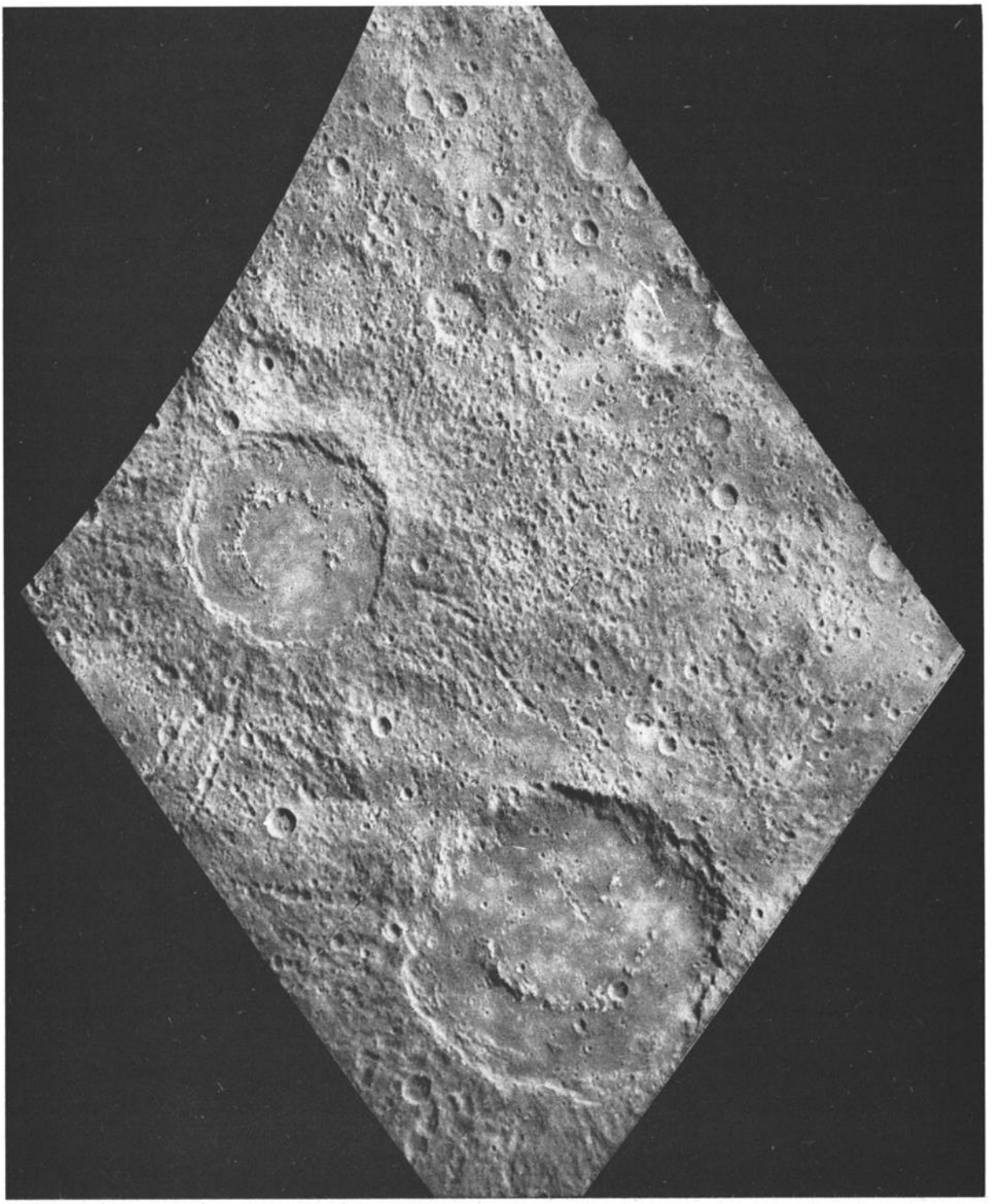

Fig. 8. Orthographic projection of craters 14 (128-km diameter) and 15 (195-km diameter) that have interior rings of mountains and ejecta deposits which are scarred by deep secondary crater chain grooves. FDS frame 150.

although (6) is appropriate for craters with less than a 10-m diameter formed in rock in the terrestrial gravitational environment [*Gault*, 1973]. For present purposes, however, (7) is appropriate to the size of craters considered in the following discussion (>1 km), and it indicates that for large craters formed with equal *KE* on Mercury (g = 370 cm/s^2) and the moon (g = 16^2 cm/s^2) the mercurian craters of excavation would be smaller in a ratio of 0.81 due to the difference in gravitational fields. However, for equal masses impacting with velocities that typically differ by a factor of 2 as suggested by *Wetherill* [1975], the 4-fold increase in *KE* would compensate for gravity effects and cause mercurian excavation craters to be larger in the ratio 1.15.

EJECTA DEPOSITS

All craters studied in this and the following sections are relatively fresh, sharp forms that are included as rayed craters, dark halo craters, or young craters with well-developed ejecta and secondary fields on the geologic map by *Trask and Guest* [1975], comparable to craters of Copernican

and Eratosthenian age on the moon or class 1 craters in the system of *Arthur et al.* [1963]. Detailed studies of the ejecta deposits of the mercurian craters have been limited to 27 structures which were selected to give as broad a coverage of crater sizes and morphologic types as possible consistent with acceptable resolution of the imagery available from the first encounter with Mercury by Mariner 10. Results from the second-encounter photography were not processed in time for this study, but they will provide a wealth of additional craters for analysis and a better statistical base for data.

Figure 1 shows the location of the 27 craters: 11 craters viewed as Mariner 10 approached Mercury and 16 craters viewed after encounter. Table 1 lists the size and latitude and longitude of these craters as a reference for other workers. It should be noted that although the western rim of crater 26, the largest selected for study, has not emerged from the morning terminator in the photomosaic shown in Figure 1, subsequent photography taken 14–24 hours later revealed its full diameter and the probable presence of a central ring similar to other mercurian structures of comparable size.

Continuous ejecta deposits. The radial extent of the hummocky facies between the crater rims and the outer limits of the radially ridged facies, the continuous ejecta deposits, was mapped on acetate sheets overlaying rectified (or original unforeshortened) pictures of the 27 craters listed in Table 1. Three individuals (D.E.G., J.E.G., and M.C.M.) mapped each crater independently and ascertained subjectively an average value for the radial extent of the continuous ejecta deposits. The averages of the three determinations are presented in Figure 9 where they are compared with similar data for lunar craters derived (by D.E.G. and J.E.G.) from lunar orbiter and Apollo imagery.

The comparison reveals that for a given rim diameter the radial extents of the lunar deposits are systematically larger than those for Mercury. For a simple linear relationship between radial extent of the continuous deposits R_c and the rim diameter D_r, least squares fits to the two sets of data give

$$(R_c/D_r)_m = 0.44 - 10^{-3}D_r \quad (9)$$

and

$$(R_c/D_r)_l = 0.68 - 1.5 \times 10^{-3}D_r \quad (10)$$

for the mercurian and lunar cases, respectively. The expressions are appropriate only for craters smaller than approximately 300 km.

Taking the ratio R_{cm}/R_{cl} for equal size craters, (9) and (10) yield mercurian ejecta deposits that are approximately 0.65 the width of lunar deposits. This reduced width of the mercurian deposits is qualitatively consistent with the relative values of the gravitational accelerations for the two bodies, but in order to make a more quantiative comparison, consider first two impact events that occur under identical conditions (i.e., material properties, impacting mass, impact velocity, etc.) with the exception that the gravity fields are different. Peak shock stresses and wave geometry will be identical for the two events, so that ejecta velocities, angles of ejection, fragment size distribution, etc., should also be identical. For this hypothetical condition the ballistic range R_{ec} of ejecta reaching the limits of the continuous deposits of the maximum extent considered in Figure 9 (<100 km) is adequately described by the simple range equation for a flat surface. On this basis the ballistic range is inversely proportional to the gravitation acceleration $R_{ec} \propto 1/g$, and ejecta comprising the outer limit of the continuous deposits on Mercury would have a range that is a factor 0.44 less than the same material would attain on the moon, a value significantly smaller than the observed value $R_{cm}/R_{cl} = 0.65$. The two values, however, are not directly comparable, since the former corresponds to total ballistic range R_e for material ejected from within an excavation crater of diameter D_e, while the latter is the distance from the rim of craters with diameters D_r to the limit of the continuous deposits; R_e is greater than R_c, and D_r may be considerably greater than D_e, depending on the amount of postcratering modifications that may have occurred. Moreover, the excavation craters D_e for the two cases will be different because of the original assumption of identical conditions (i.e., *KE*) except for gravity fields.

The comparison improves if the hypothetical conditions are

TABLE 1. Location and Size of Craters Used for Continuous Ejecta Blanket Measurements

Crater	Latitude, deg	Longitude, deg	Rim Diameter, km
1	−15.95	16.03	120
2	21.02	18.27	240
3	20.14	21.51	120
4	10.74	21.24	88
5	0.41	23.74	90
6	6.31	14.44	59
7	0.08	20.15	20
8*	−10.94	31.48	63
9	−16.72	28.25	14
10	−39.60	31.52	106
11	−44.96	18.42	27
12	65.60	170.33	140
13	61.15	138.81	70
14	59.41	127.56	128
15	54.51	136.38	195
16	59.53	178.26	98
17	50.20	178.54	74
18	37.86	126.17	54
19	31.40	176.10	77
20	25.65	180.32	60
21	9.60	133.54	90
22	3.55	138.59	120
23	−1.83	146.47	126
24	9.77	169.45	48
25	9.12	174.11	49
26	8.19	189.64	250
27	−31.07	168.91	70

Location of craters is according to the Mariner 10 surface coordinate system [*Davies and Batson*, 1975].
* Crater Kuiper [*Murray et al.*, 1974*b*].

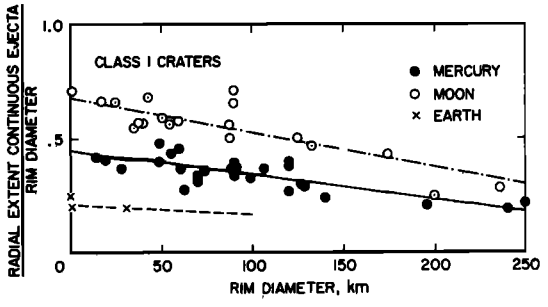

Fig. 9. Average radial extents of continuous ejecta deposits around fresh class 1 craters for Mercury, the moon, and earth. Lines through mercurian and lunar data points are least squares fits to measurements; earth data points are based on Ries basin, Germany, Meteor Crater, Arizona, and laboratory hypervelocity (6-7 km/s) impact craters formed in noncohesive sand. See text for discussion of line through terrestrial data points.

now changed by increasing the size (KE) of the impacting body which impacts the surface with the higher value of gravitational acceleration. The relative wave geometry will remain the same and scale up directly with the size of the impacting body; the new excavation diameter D_e will increase according to (7), and the absolute position of the effective point of ejection of material from within the enlarged excavation crater will be moved radially outward. When the ratio R_e/D_e is now formed by using β as the exponent for the scaling relationships in (6), (7), and (8),

$$R_e/D_e \propto g^{\beta-1} \tag{11}$$

and the mercurian-lunar ratio R_{em}/R_{el} for equal values of D_e becomes 0.54 in better agreement with the observations R_{cm}/R_{cl}. This larger value, however, is still not directly comparable to the observations because for the general conditions represented in Figure 9, postcratering modifications have occurred (i.e., $D_r > D_e$, as will be shown later in the section on interior structures), and there is evidence that the increase in diameter for a given initial value of D_e is not the same for Mercury and the moon.

Perhaps a potentially more meaningful comparison can be made by writing the range R_e in terms of R_c. By introducing the incremental increase in diameter ΔD due to postcratering modifications and a constant $0 < n < 0.5$ which defines the position within the excavation crater at which the ejecta effectively leaves the crater,

$$R_e = R_c + nD_e + \Delta D \tag{12}$$

For $n = 0$ the ejecta is considered to leave the excavation crater at its rim; for $n = 0.5$ the ejecta would originate from the center of the crater. The ratio R_{cm}/R_{cl} can then be obtained in the form

$$\frac{R_{cm}}{R_{cl}} = \frac{D_{em}(R_e/D_e - n - \Delta D/D_e)_m}{D_{el}(R_e/D_e - n - \Delta D/D_e)_l} \tag{13}$$

Because values for ΔD are unknown, consider only those smaller craters ($D < 10$ km) for which $\Delta D = 0$, so that $D_e = D_r$ and $D_{em} = D_{el}$, and recast the ratio into

$$\frac{R_{cm}}{R_{cl}} = \frac{(kg^{\beta-1} - n)_m}{(kg^{\beta-1} - n)_l} \tag{14}$$

where k would be the constant of proportionality in (11). Because $D_{em} = D_{el}$, this approximation effectively assumes from (7) that $KE_m = (g_m/g_l)KE_l$; for impacting bodies of the same mass this would correspond to conditions where the impact velocity against Mercury would be a factor of 1.5 greater than on the moon.

For the limiting condition $n = 0$, (14) gives the same result as (11) (i.e., $R_{cm}/R_{cl} = 0.54$), and for $n > 0$ the value n_m for Mercury must be less than the value n_l for the moon if the ratio R_{cm}/R_{cl} is to be greater than 0.54. Without some knowledge of the value of the proportionality constant k, however, the appropriate values for n to achieve or approach a value of the ratio of 0.65 cannot be obtained. On the other hand, if the fraction of the total ejecta mass that is contained within the continuous deposits can be estimated, values for n can be derived, and possibly some evaluation of the proportionality constant k can be obtained—a potentially important approach for future studies to determine scaling laws of large impact events.

Secondary impact craters. Secondary impact craters were mapped onto clear acetate sheets overlying photographically enlarged and computer-rectified pictures of three primary mercurian craters and then counted in concentric annuli around the primary structures. Four lunar craters were similarly mapped by using lunar orbiter and Apollo photographs. Figure 10 presents a map for mercurian crater 12. Because of the difficulty in distinguishing between secondary craters and small primary impact craters near the resolution limit of the pictures, all craters with diameters greater than an arbitrary lower limit are included in the counts (0.014 of the primary rim diameter). However, for the lunar craters Aristarchus, Copernicus, and Harpalus [*Murray*, 1972], secondary craters could be distinguished with considerable confidence on the basis of the lunar orbiter and Apollo imagery. Thus while the lunar counts are probably most representative of the actual secondary crater populations, the counts for Tsiolkovsky and the mercurian craters may include some superposed primary craters. In all cases, many of the small craters in the pictures are difficult to differentiate from hollows and depressions of other origins, particularly in the rough hummocky terrains near the primary craters; counts on all seven craters were done by one individual (J.B.M.), so that results presented herein are subjectively consistent.

Only the secondary crater counts for crater 12 are complete. Due to its proximity to the evening terminator, crater 1 is poorly illuminated on its eastern side, and counts for only the western side could be accomplished. Only counts to the east of crater 19 have been completed by January 1975. For all three mercurian craters, other large primary craters were in relatively close proximity. Some of these craters had fields of secondaries close to the field under study; where these areas could be identified, they have been excluded from the counts presented here.

Results of the secondary crater counts (Figures 11 and 12) confirm the general impression gained from visual inspection and comparisons of mercurian and lunar craters; the areal density of the mercurian secondary crater population is greatly enhanced over those for the lunar craters. However, the general trends of the secondary populations both on Mercury and on the moon are very similar. With increasing distance

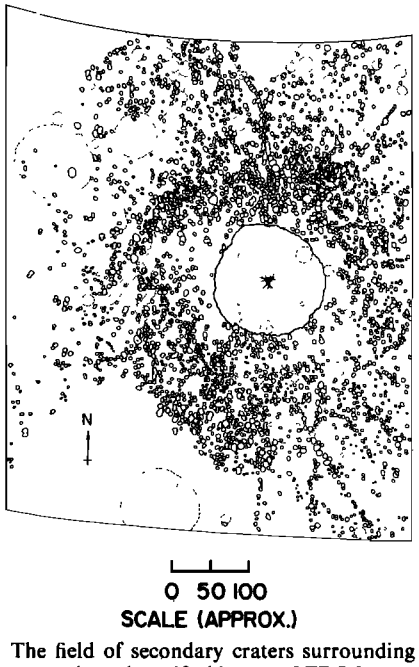

Fig. 10. The field of secondary craters surrounding crater 12 as mapped from an enlarged rectified image of FDS frame 166 shown in Figure 3.

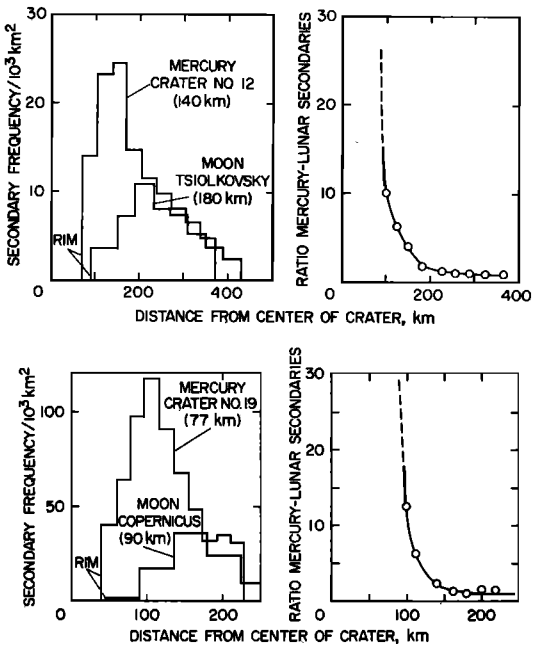

Fig. 11. Radial variations in the areal density of secondary craters and the ratios of mercurian to lunar secondary craters for Mercury craters 12 and 19 and for lunar craters Copernicus and Tsiolkovsky.

from the crater rims the areal density of secondary craters increases rapidly to a maximum value and then decreases more slowly over a distance of several crater diameters to values less than those at the rim. The increase in density with distance from the rim is most rapid for the mercurian craters, but the position of maximum density, both for Mercury and for the moon, occurs outside limits previously determined for the rim facies comprising the continuous ejecta deposits, a result consistent with the distinction made between an inner rim facies and an outer zone of satellitic craters.

The maximum values of areal density for the secondary crater populations increase with decreasing diameter of the primary crater, but this is an apparent result caused by the arbitrary limitation invoked to limit the secondary crater counts to craters larger than $0.014D_r$. Thus the cutoff for Aristarchus and Tsiolkovsky occurs for craters of 0.5-km and 2.5-km diameter, respectively, and would correspond to a factor between 10 and 10^2 decrease in the relative crater population for the latter. Comparison of the secondary crater populations between Mercury and the moon therefore must be made for craters of approximately the same size. Toward this end the secondary crater counts for craters 12 (140 km) and 19 (77 km) are compared in Figure 11 with approximate dimensional analogues in the lunar environment, Tsiolkovsky (180 km) and Copernicus (90 km). Although the craters do not have the same rim diameters, all four craters have experienced postcratering enlargement of their excavation diameters due to slumping of the interior walls as indicated by terracing. The incremental changes are rather uncertain, particularly for Tsiolkovsky, whose interior structure has been modified by endogenetic processes [*Guest and Murray*, 1969], but it is estimated that the excavation craters 12 and 19 have been enlarged by about 30 and 13 km, respectively, and *Shoemaker* [1962] suggests that there has been at least a 25-km increase in the diameter of Copernicus due to slumping. Crater 19 and Copernicus therefore provide a comparison for craters with transient diameters D_e of about 65 km, and crater 12 and Tsiolkovsky are comparable for diameters between 110 and 140 km(?) if the Tsiolkovsky has experienced changes in its diameter proportional to those of crater 19.

For the two pairs of primary craters (Figure 11) the radial variations and numerical values for the ratio of mercurian to lunar secondary craters are virtually identical. The ratios are greatest (>10) nearest to the crater rims and are clearly related to the difference in the extents of the continuous ejecta deposits; the mercurian deposits are narrower and evolve into the secondary crater fields closer to the rim than in the case of lunar craters. The ratios decrease rapidly, however, with increasing distance from the rim, as the crater counts are based upon the populations of both secondary fields. Values of about 1 are attained at a distance of approximately two crater diameters from the rims of the excavation craters and thereafter remain essentially constant or continue to decrease slowly for another crater diameter, the radial limit of the data.

The greatly enhanced areal density of mercurian secondaries relative to lunar populations is explicable, again, in terms of the differences in the gravitational constants of the two bodies. Qualitatively, the reduced ballistic range on Mercury acts to reduce the dispersion between individual ejecta fragments producing secondaries and serves to concentrate them into smaller areas circumscribing the point of the impact. The net effect leads to a greater number of secondaries being formed per unit area. In this connection the long linear crater form grooves (Figure 3) are a result of this reduced dispersion for the large secondary ejecta masses; in a lower gravitational field the secondary craters would not overlap each other but, instead, would produce a chain of discrete craters.

It should be cautioned, however, that for both comparisons shown in Figure 11 the mercurian rim diameters D_r are less than their lunar counterparts. Because of the arbitrary cutoff in the counts of secondary craters at a size $0.014D_r$, numerous smaller secondaries have been included in the mercurian counts that have been excluded from the comparable lunar data. This exclusion will serve to increase the mercurian secondary crater frequency relative to the moon by an unknown amount. For this reason it is instructive to consider a simple model for estimating the effect of concentrating mercurian

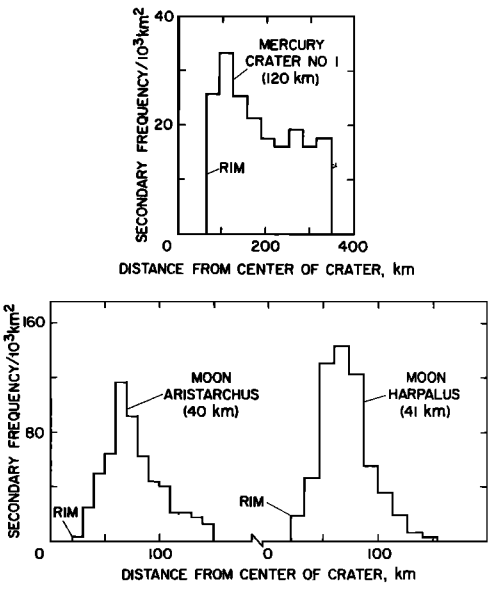

Fig. 12. Radial variations in areal density of secondary craters for Mercury crater 1 and lunar craters Aristarchus and Harpalus.

secondaries into smaller circumscribing areas around the primary crater.

For this application the ballistic range equation for a spherical body is required because the maximum range of the data (400 km) exceeds the limits for a flat surface approximation. Figure 13 presents the ratio of mercurian to lunar ballistic range as a function of the ejection velocity for two representative values of the angle of ejection, which includes the values suggested by laboratory impact experiments [*Gault et al.*, 1963; *Gault et al.*, 1968; *Stöffler et al.*, 1975]. The ratio is relatively constant (0.44) and insensitive to ejection angle up to velocities of about 0.5 km/s (mercurian range ~ 60 km; lunar ~ 150 km) but decreases significantly for the higher velocities, especially for the more shallow angle(s) of ejection. Velocities of about 1.2 km/s are necessary for the 400-km range on Mercury.

Now, if we consider two craters of approximately the same size, as discussed previously, then the population of the fragmental material producing secondary craters and the conditions for ejection from the primary craters will be similar, and the family of mercurian secondary craters will impact the surface in concentric rings closer to their source, as shown by Figure 13. The effective reduction in the reference area A_r for the population at a given range R_e will be inversely proportional to the radial distance from the crater center, or in terms of D_e and n,

$$A_r \propto [R_e + (0.5 - n)D_e]^{-2} \tag{15}$$

Appropriate values for n will approach 0.5 because the material ejected at the highest velocities originates closest to the impacting body at the center of the crater. For this reason, when R_e is larger than D_e by a factor of more than 2 or 3, (15) may be approximated as $A_r \propto R_e^{-2}$, and the areal density of the mercurian secondary craters compared to densities for the moon will be increased by the ratio

$$\frac{A_{rm}}{A_{rl}} = \left[\frac{R_{el}}{R_{em}}\right]^2 \tag{16}$$

Numerical values for the areal density ratio, based on Figure 13, are presented in Figure 14 and mirror the range ratios. The areal density of mercurian secondary craters is approximately 5 times greater than that for the moon for the shorter ranges corresponding to ejection velocities less than about 0.5 km/s, but the ratio increases rapidly for velocities in excess of about 1 km/s. For the extreme range of 400 km for the comparison shown in Figure 10 the secondary crater ratio would be between 7 and 9, depending on the angle of ejection from the crater. Within the constraints of the crater count data and the simplified model used to correct for the differences in the gravitational acceleration, the measured and calculated values of the enhancement of mercurian secondary crater population are in reasonable agreement only at the outer limits of the continuous deposits. Beyond about two crater diameters from the rims, however, the simple model grossly overestimates the ratio even though the basic data are biased toward some enhancement of the mercurian secondary crater population. The oversimplification of the model would be first suspect for the disagreement, but one cannot discount the possibility that a fundamental assumption behind the model is not valid, in particular, that the material properties and fragment size distributions from lunar and mercurian craters are similar. Further studies and comparisons are required to substantiate these numerical results, but the qualitative effects of increased gravity compressing and restricting mercurian secondaries into a narrower ring around the point of impact seem adequately confirmed.

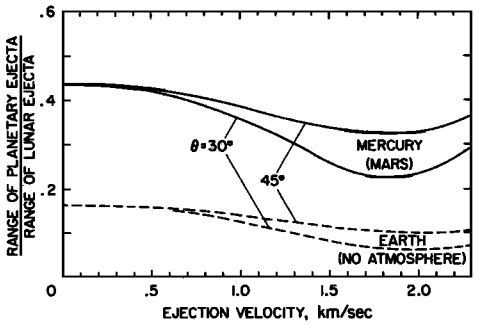

Fig. 13. Calculated ballistic range for ejecta on atmosphere-free bodies relative to the range on the moon as a function of ejection velocity and angle of ejection θ measured with respect to the local horizontal.

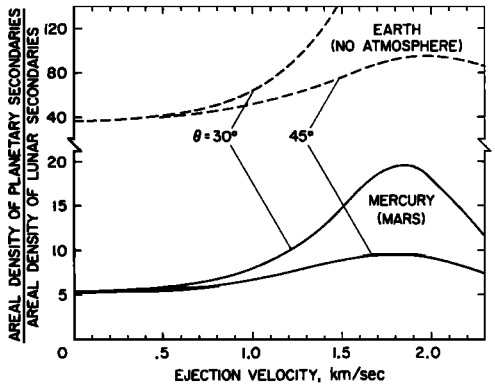

Fig. 14. Calculated areal density of secondary craters for atmosphere-free bodies relative to the moon, based on values of ballistic range given in Figure 13. See text and (16).

INTERIOR STRUCTURE

As the basis for quantitative comparisons of the interior structures of mercurian and lunar craters, 130 mercurian craters were selected for depth-diameter determinations and the occurrence of terracing and central peak(s). This group of craters includes many of those listed in Table 2 and is essentially randomly distributed with respect to planetary latitude, but they cluster within approximately 20° longitude of the morning and evening terminators in order to obtain shadows which are useful for the measurements. All craters correspond to class 1 features in the system of *Arthur et al.* [1963] based on the subjective judgment of the degradational state indicated by the crispness of the rim and interior structures and the freshness of the continuous ejecta deposits and/or secondary crater fields. Depth-diameter calculations from shadow length analysis are based on the best spacecraft trajectory and camera-pointing information available in January 1975; limited by the quality of the supporting data, the reliability of the measurements is estimated to be better than 10%.

Depth-diameter relationships. Results from the mercurian depth-diameter measurements are presented in Figure 15, where they are compared with *Pike*'s [1974*a*] most recent photogrammetric determinations for lunar craters. Although the available resolution of the Mariner 10 photography restricts the data for the mercurian results to craters larger than 1 km, it is nevertheless apparent that the trend of the depth-diameter relationship for craters on Mercury is

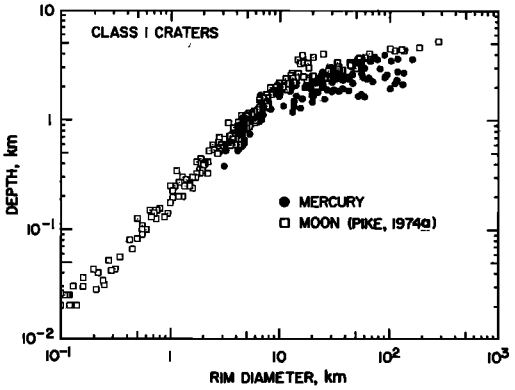

Fig. 15. Comparison of the depth-diameter relationship for fresh mercurian and lunar craters.

remarkably similar to that for the moon. There is a pronounced kink in the mercurian data set at diameters between 5 and 10 km in a manner similar to that for the moon at diameters around 15 km. For diameters less than, say, 7–8 km the mercurian craters appear to have a depth-diameter relationship very nearly identical to that of the moon; for diameters greater than 7–8 km the mercurian craters are systematically shallower than their lunar counterparts, but they do follow a trend almost parallel to that for the moon.

If we follow the procedure of *Pike* [1974*a*] and divide the mercurian data set into two groups, a least squares fit for diameters less than 7 km (the diameter that yields minimum residuals) gives

$$d = 0.15D_r^{1.09} \quad (17)$$

and for diameters greater than 7 km

$$d = 0.93D_r^{0.27} \quad (18)$$

where d and D_r are, respectively, the depth and rim diameter in kilometers. For lunar craters, *Pike* [1974*a*] gives for craters less than about 15 km, in the same notation,

$$d = 0.196D_r^{1.010} \quad (19)$$

and for diameters greater than about 15 km

$$d = 1.044D_r^{0.301} \quad (20)$$

The strong similarity between the two suites of data is evidenced by the degree of agreement in the least squares solutions. Over the range of the mercurian measurements, (17) yields values 15–20% lower than (19), and (18) gives values 25–30% lower than (20). Direct comparisons, however, should be made with caution. *Pike* [1974*a*] points out that photogrammetric results yield more accurate results than shadow techniques and in general give slightly greater depths. Differences between the two methods are most pronounced for the smaller craters below the kink in the data. Thus it appears possible, if not probable, that the differences between (17) and (19) are caused either totally or in part by technique differences in depth determinations, while the differences expressed between (18) and (20) are real and represent the effect(s) of differences in their cratering environments. In support of this interpretation, independent of the precise numerical fits to the depth-diameter data, is the observation that the kink in the mercurian depth-diameter relationship occurs over a range of crater diameters that is approximately a factor of 2 less than for lunar craters. This is consistent with the ratio of their respective gravitational accelerations (in centimeter gram second units, 370/162 = 2.3) and with the suggestion [e.g., *Shoemaker*, 1962; *Quaide et al.*, 1965; *Gault et al.*, 1968] that postcratering slumping of crater walls is induced by gravitational forces and leads to interior terracing and perhaps central peaks. Slumping would serve to decrease depths of craters relative to their diameters, and most importantly, slumping would be expected to first occur for some critical size of crater for which the induced lithostatic stresses with increasing diameter would exceed the local material strengths around and under the transient excavation crater, thus precipitating slope or base type failures [*Varnes*, 1958; *Mackin*, 1969]. If such an interpretation is valid, then terraces and central peaks on Mercury also should occur at smaller diameters than on the moon. Accordingly, the frequency of their interior structures as a function of crater diameter is considered in the following section.

Terrace and central peak frequency. Figure 16 and Tables 2 and 3 present the frequency of terraced and central-peaked mercurian craters for the same sample of 130 craters used for depth-diameter determinations. Similar data reported by *Smith and Sanchez* [1973] for lunar craters are shown for comparison, and it is evident that both terraces and central peaks do occur in smaller craters on Mercury than on the moon. For Mercury, 80% of the 10- to 20-km diameter size class craters are terraced, and effectively all craters larger than 20 km are terraced; only 2 out of 71 craters (3%) larger than 20 km did not have terraces. In contrast, only 12% of the 10- to 20-km size class of lunar craters are terraced, and complete terracing (equivalent to the mercurian 3%) is not attained until crater diameters are greater than 40 km, twice the size that is required on Mercury.

Comparable results also are found for central peaks. For Mercury, 80% of the 10- to 20-km size craters exhibit central peaks, while only 5 out of 71 (7%) with diameters larger than 20 km do not have peaks. On the moon, the Smith and Sanchez results give 26% peaked in the 10- to 20-km size class, and complete 'peakism' equivalent to complete terracing does not occur until craters are between 30- and 40-km diameter, again almost twice the size of their lunar counterparts. Moreover, if allowances are made between the two data sets for the differences in (1) the resolution between Mariner 10 imagery and the lunar orbiter and Apollo photography available to Smith and Sanchez, and (2) their interpretation and definition of central peaks, the contrast between Mercury and the moon in the frequency of central peaks is even greater (see Table 3).

An additional comparison of the interior structures is afforded by the results shown in Figure 17, where the progression with crater size from the occurrence of simple central peak to concentric ringed complexes is given for Mercury. In

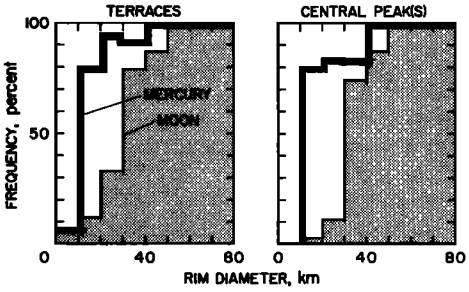

Fig. 16. Comparison between Mercury and the moon for the frequency of occurrence of terraces and central peaks as a function of crater rim diameter. Lunar data from *Smith and Sanchez* [1973].

TABLE 2. Comparison of Terrace Frequency for Mercurian and Lunar Craters

Rim Diameter, km	Mercury			Moon*		
	Total Number	Number Terraced	Percent Terraced	Percent Terraced	Number Terraced	Total Number
0–10	43	3	7	0	0	6
10–20	25	20	80	12	4	34
20–30	19	18	95	33	7	21
30–40	12	11	92	79	15	19
40–50	7	7	100	87	7	8
50–60	11	11	100	100	7	7
60–120†	22	22	100	100	20	20

* From Smith and Sanchez [1973].

† 140 km for the moon.

general the mercurian craters smaller than about 100-km diameter are characterized by a single peak or a complex of multiple peaks. Beginning at diameters of about 100 km, however, ringed structures of peaks, concentric with the main crater rim, also occur; the limited data sample available indicates that the central peaks disappear between 130- and 180-km diameter and only craters having an inner ring of peaks occur for diameters greater than 180 km. This progression is strikingly similar to that for the moon [*Stuart-Alexander and Howard*, 1970; *Hartmann*, 1972]. Between about 150- and 300-km diameter they point out that craters have either central peaks or rings, but above 300 km, all structures are ringed, a size that again is approximately twice its mercurian morphologic equivalence. It might be noted that based on their observations, Stuart-Alexander and Howard defined lunar basins to have diameters greater than 300 km, and perhaps a comparable criterion of 150 km would be appropriate for the definition of basins on Mercury.

The results presented in Figures 15, 16, and 17, taken collectively, indicate that the factor of 2.3 difference in the gravitational environments of Mercury and the moon is mirrored by the approximate factor of 2 difference between the two bodies for the onset of the change in their depth-diameter relationships and the occurrence of terraces, central peaks, and ringed basins. Moreover, the role of gravity is also suggested in the recent results reported by *Wood* [1973], who found that the heights of central peaks are directly proportional to crater diameter. Although Wood concludes that the linear proportionality implies that peak height is a function of crater-forming energy, we suggest that the linear proportionality is instead the result of the gravitational potential energy that is expended as the transient excavation craters collapse after they attain their maximum dimensions. As discussed earlier, crater dimensions are a function of energy, but the functional relationship is not linear. On the other hand, gravitational potential energy available by collapse of a crater should scale directly and linearly with the depth of the transient excavation cavity. If this interpretation is correct, one would expect central peak heights on Mercury to be approximately twice as high as lunar peaks for the same size craters. Preliminary Mercury data, however, are almost identical with those of the moon, but *Wood*'s [1973] limited data for heights of central uplifts (peaks?) of terrestrial craters support the argument. *Wood* [1973, equations 5 and 6] gives (with h the height and all dimensions in kilometers)

$$h = 0.026D_r - 0.26 \quad (21)$$

$$h = 0.13D_r - 0.23 \quad (22)$$

for lunar and terrestrial craters, respectively. The change in the heights with diameter is a factor of 5 greater for earth than for the moon (0.13/0.026 = 5). With consideration of the limitations in the terrestrial data the factor of 5 is in remarkably good agreement with the actual ratio of 6 for the gravitational accelerations for the two bodies.

Although we cannot exclude the possibility that what appears to be remarkably consistent effects of gravitational acceleration may be, instead, the sum of multiple effects and events, the suggestion by *Shoemaker* [1962], *Quaide et al.* [1965], *Gault et al.* [1968], and many others that the phenomena under consideration are the end product of processes driven by gravitational forces seems more than adequately confirmed.

TABLE 3. Comparison of Central Peak Frequency for Mercurian and Lunar Craters

Rim Diameter, km	Mercury			Moon*		
	Total Number	Number With Peak(s)	Percent Peaked	Percent Peaked	Number With Peak(s)	Total Number
0–10	43	0	0	0	0	5
10–20	25	15	80	26 (3)†	8 (1)	31
20–30	19	16	84	53 (11)	10 (2)	19
30–40	12	10	83	79 (74)	15 (14)	19
40–50	7	7	100	87	7	8
50–60	11	11	100	100	7	7
60–120§	22	22	100	100	20	20

* From *Smith and Sanchez* [1973].

† Estimated for photographic resolution and interpretation comparable to Mariner 10 imagery (see text).

§ 140 km for the moon.

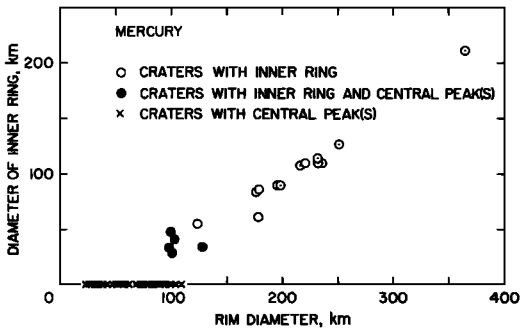

Fig. 17. Changes in the interior structure of mercurian craters and their inner ring diameter as a function of the outer (rim) diameter.

Concluding Remarks

These comparisons between mercurian and lunar impact craters, taken collectively, clearly indicate important differences in the two populations of craters. The differences are attributable to differences in the gravity fields, but whether or not they are the direct and sole effects of the gravitational environments cannot be determined. The degree of correlation that is obtained based on assuming only gravitative effects is more than adequate, however, to assure that gravitational acceleration has been the primary agent for the observed differences. Imagery for fresh craters formed in different gravity fields would be ideal for further studies, and although the other terrestrial bodies are unsuited for this purpose, possibly future photography of the satellites of the major planets will provide additional observational data.

Notwithstanding some reservations, it is interesting to consider further the depth-diameter data as applied to terrestrial craters. The kinks or changes in the depth-diameter relationships occur both on Mercury and on the moon for diameters slightly less than the beginning of the range of sizes over which terracing and central peaks become abundant. For Mercury the kink is between 5 and 10 km; only 7% of the craters less than 10 km are terraced, but in contrast 80% of the 10- to 20-km size class are terraced and peaked. In the case of the moon with its kink at about 15 km, 12% of the 10- to 20-km size class are terraced, and it is only for craters larger than 30-km diameter that terraces and central peaks become common at the 80% level. Thus it appears that for crater sizes below the change in the depth-diameter relationship the crater geometry is determined by the excavation processes and depth-diameter ratios are effectively independent of gravity, consistent with laboratory impact cratering results [*Gault and Wedekind,* 1975]. For crater sizes above the change the excavation geometry is modified by postcratering collapse of the rim structure with a consequent increase in diameter and decrease in depth. Extrapolation of this interpretation to terrestrial craters formed in a gravitational field about 3 times greater than on Mercury leads to the expectation that a similar kink occurs for diameters 1–3 km on earth and is accompanied by terracing and central peaks. This expectation is in general agreement with known impact structures and implies that the relatively low relief of the larger terrestrial craters is the result of gravity-induced postcratering processes in addition to long-termed erosional effects.

Some further support for the greater effects of gravity on earth is shown in Figure 9, where three data points for the radial extent of the continuous ejecta deposits are compared with the mercurian and lunar determinations. The terrestrial data are estimates from maps of Meteor Crater, Arizona [*Shoemaker,* 1963] and the Ries basin [*Hüttner et al.,* 1969], the third datum being based on small (30-cm diameter) hypervelocity impact craters formed in sand at an ambient pressure of less than 1 torr (D. E. Gault, unpublished data, 1974). The three data points fall well below the values for Mercury. Extrapolation of the mercurian least squares fit to terrestrial gravity, in proportion to the moon-Mercury ratio, yields the dashed line in good agreement with the data points. It is to be noted that Figure 13 predicts a smaller value (0.16) than the observed values (~0.2) in Figure 9 in the same manner that the Figure 13 underestimates (0.44) the observed value for Mercury (0.54) in Figure 9. It should be anticipated, moreover, that the secondary crater population should be greatly enhanced over the crater populations of Mercury and the moon, especially at the limit of the continuous deposits (Figure 14).

The significance of the mercurian-lunar comparisons is not restricted to the interpretation of craters on other planetary bodies. *Trask and Guest* [1975] point out that the most widespread surface unit on Mercury, mapped as an intercrater plains unit, is a flat or gently rolling terrain between large craters and basins. This unit is heavily cratered with small craters and is analogous to small areas on the Moon in pre-Imbrian plains. Trask and Guest postulate that the mercurian intercrater plains are an ancient primordial surface whose lunar analogue has been largely obliterated because of the moon's greater number of subsequent large craters and basins [*Murray et al.,* 1974*b*]. An additional reason, perhaps of more importance, is that the greatly reduced ballistic range of ejecta on Mercury relative to the moon would reduce the effectiveness of large events in obliterating and/or modifying extensive areas on the mercurian surface.

It should be noted that the observed reduction in the ballistic transport of ejecta on Mercury relative to the moon has important implications for two recent analyses which developed models of the radial thickness distributions of ejecta around lunar craters, with particular emphasis on and application to the large basins Orientale and Imbrium [*McGetchin et al.,* 1973; *Pike,* 1974*b*]. The models depend critically on an evaluation of (1) the thickness of the deposits on the rim of the excavation crater and (2) the functional relationship used to describe the change in thickness with distance from the rim. Although Pike corrects several important shortcomings in the McGetchin et al. analysis, both modeling studies are based on data from terrestrial craters, and empirical representations for the rim thickness and radial decay are derived with no corrections for the difference in gravitational environments between the earth and the moon. Figure 9, 13, and 14 clearly indicate that lunar rim deposits should be significantly thinner than terrestrial deposits for any given size excavation crater. Moreover, it is not certain that the functional expression for the radial change in thickness with distance from the rim is independent of gravity. The subject is beyond the scope of this discussion, but it is cautioned that the difference between lunar and terrestrial rim deposits cannot be as great as indicated by Figure 14, because the assumptions behind (16) are not valid for the conditions $R_e \ll D_e$ being considered here. It is, perhaps, sufficient to note here only that the expressions for ejecta thicknesses presented by *McGetchin et al.* [1973] and *Pike* [1974*b*] are poorly based and require major revisions to account for gravitational differences between the earth and the moon.

The obliterating effect of ejecta from large basin-forming events at great distances from the point of impact has par-

ticular significance for the moon and is emphasized by the measurements of the continuous deposits shown in Figure 9. Although these data do not extend up to dimensions of the order of the Orientale and Imbrium events, the results nevertheless indicate that their continuous deposits would certainly be no greater than $0.25D_r$. If D_r is defined by the outer ring for these basins, then the radial extents of the continuous deposits would be no greater than 200 or 300 km, respectively, from the arcs described by the Cordillera and Apennine mountains. If an inner ring is used as a reference value for D_r, the radial extents would be contained within these same arcs. Thus the margins of the continuous deposits for these basins are restricted to distances no greater than about 650 km from the center of the Orientale basin and about 900 km for Imbrium; secondary crater fields must extend beyond these distances, a conclusion that is consistent with and supports the argument of *Oberbeck et al.* [1974] that secondary cratering and the associated mixing of ejecta with local material occur at such distances rather than the deposition of a discrete layer of ejecta from the basin. On this basis the radial lineations described as Imbrium sculpture at distances of more than 1000 km from the outer ring cannot be part of a 'continuous' deposit. By analogy, the continuous deposits surrounding Caloris Planitia must have an even more restricted radial extent, and the greater portion of the circumscribing terrain represents the secondary crater field from Caloris. Because of almost identical gravitational fields, it seems reasonable that Caloris Planitia provides a remarkable analogue for the great basin Hellas on Mars before degradation to its current eroded state. Indeed, the fresh mercurian craters should be models for all martian impact craters; the absence of fresh structures and the degraded morphology of craters on Mars constitute mute evidence for the effectiveness of eolian erosion and deposition and indicate the inadequacy of martian craters for assessing morphologic characteristics of cratering processes.

Acknowledgments. We are indebted to many individuals, but special acknowledgment must be made to the members of the Image Processing Lab of the Jet Propulsion Laboratory, in particular J. Mosher, J. Soha, and J. Lorre, for the special processing and rectification of images required for this study, to our colleagues on the Mariner 10 TV Imaging Team, B. Hapke, B. Murray, R. Strom, and N. Trask, for valuable discussions and criticism, to M. Davies for his expeditious cooperation in providing the planetary coordinates necessary for picture rectification, and to E. Danielson and K. Klausen for their sustained support of these studies. Acknowledgment is also due P. Schultz and P. Cassen for helpful discussions, R. Hayes for data reduction, R. J. Pike for providing tabulations of his depth-diameter data, and R. B. Baldwin, W. K. Hartmann, and C. R. Chapman for their careful reviews of the text. Two of us (D.D. and M.C.M.) were supported under NASA grant NGR 05-002-117 from the Planetology Program Office. The work of J.E.G. was supported by the U.K. Natural Environment Research Council. Contribution 2581, Division of Geological and Planetary Sciences, California Institute of Technology, Pasadena, California 91125.

REFERENCES

Arthur, D. W. G., A. P. Agnierary, R. A. Howath, C. A. Wood, and C. R. Chapman, The system of lunar craters, *Commun. Lunar Planet. Lab., 2,* 71–78, 1963.

Baldwin, R. B., *The Measure of the Moon,* University of Chicago Press, Chicago, Ill., 1963.

Braslau, D., Partitioning of energy in hypervelocity impact against loose sand targets, *J. Geophys. Res., 75*(20), 3987–3999, 1970.

Chabai, A. J., On scaling dimensions of craters produced by buried explosives, *J. Geophys. Res., 70*(20), 5075–5098, 1965.

Davies, M. E., and R. M. Batson, Surface coordinates and cartography of Mercury, *J. Geophys. Res., 80,* this issue, 1975.

Gault, D. E., Saturation and equilibrium conditions for impact cratering on the lunar surface: Criteria and implications, *Radio Sci., 5*(2), 273–291, 1970.

Gault, D. E., Displaced mass, depth, diameter, and effects of oblique trajectories for impact craters formed in dense crystalline rocks, *Moon, 6,* 32–44, 1973.

Gault, D. E., and E. D. Heitowit, The partitioning of energy for impact craters formed in rock, in *Proceedings of the Sixth Hypervelocity Impact Symposium,* vol. 2, pp. 419–456, Firestone Rubber Company, Cleveland, Ohio, 1963.

Gault, D. E., E. M. Shoemaker, and H. J. Moore, Spray ejected from the lunar surface by meteoroid impact, *NASA Tech. Note D-1767,* 1963.

Gault, D. E., W. L. Quaide, and V. R. Oberbeck, Impact cratering mechanics, in *Shock Metamorphism of Natural Materials,* edited by B. M. French and N. M. Short, pp. 87–99, Mono, Baltimore, Md., 1968.

Guest, J. E., Stratigraphy of ejecta from the lunar crater Aristarchus, *Geol. Soc. Amer. Bull., 84,* 2873–2894, 1973.

Guest, J. E., and J. B. Murray, Nature and orgin of Tsiolkovsky crater, lunar farside, *Planet. Space Sci., 17,* 121–141, 1969.

Guest, J. E., and J. B. Murray, A large scale surface pattern associated with the ejecta blanket and rays of Copernicus, *Moon, 3,* 326–336, 1971.

Hartmann, W. K., Interplanet variations in scale of crater morphology—Earth, Mars, moon, *Icarus, 17,* 707–713, 1972.

Hartmann, W. K., and C. A. Wood, Moon-origin and evolution of multi-ringed basins, *Moon, 3*(1), 3–78, 1971.

Hüttner, R., H. Schmidt-Koler, and W. Treibs, Ammerkungen zur Geologischen Übusichtskarte (Beilage 1), *Geol. Bavarica, 61,* 451–454, 1969.

Johnson, S. W., J. A. Smith, E. G. Franklin, L. K. Moraski, and D. J. Teal, Gravity and atmospheric pressure effects on crater formation in sand, *J. Geophys. Res., 74*(20), 4838–4850, 1969.

Lampson, C. W., Explosions in earth, in *Effects of Impact and Explosion,* vol. 1, part 2, chap. 3, p. 110, Office of Scientific Research and Development, Washington, D. C., 1946.

Mackin, J. H., Origin of lunar maria, *Geol. Soc. Amer. Bull., 80,* 735–748, 1969.

McGetchin, T. R., M. Settle, and J. W. Head, Radial thickness variation in impact crater ejecta: Implications for lunar basin deposits, *Earth Planet. Sci. Lett., 20,* 226–236, 1973.

Murray, J. B., The geology and geomorphology of the Aristarchus plateau region of the moon, Ph.D. thesis, Univ. of London, London, 1972.

Murray, B. C., M. J. S. Belton, G. E. Danielson, M. E. Davies, D. E. Gault, B. Hapke, B. O'Leary, R. G. Strom, V. R. Soumi, and N. Trask, Mariner 10 pictures of Mercury: First results, *Science, 184*(1307), 459–461, 1974*a*.

Murray, B. C., M. J. S. Belton, G. E. Danielson, M. E. Davies, D. E. Gault, B. Hapke, B. O'Leary, R. G. Strom, V. R. Soumi, and N. Trask, Mercury's surface: Preliminary description and interpretation from Mariner 10 pictures, *Science, 185*(4146), 169–179, 1974*b*.

Murray, B. C., R. Strom, N. J. Trask, and D. E. Gault, Surface history of Mercury: Implications for terrestrial planets, *J. Geophys. Res., 80,* this issue, 1975.

Oberbeck, V. R., and R. A. Morrison, The lunar herringbone pattern, *NASA Spec. Publ. 330,* section 32, pp. 15–29, 1973.

Oberbeck, V. R., R. H. Morrison, F. Hörz, W. L. Quaide, and D. E. Gault, Smooth plains and continuous deposits of craters and basins, *Geochim. Cosmochim. Acta., 1,* 111–136, 1974.

Pike, R. J., Depth/diameter relations of fresh lunar craters: Revision from spacecraft data, *Geophys. Res. Lett., 1*(7), 291–294, 1974*a*.

Pike, R. J., Ejecta from large craters on the moon: Comments on the geometric model of McGetchin et al., *Earth Planet. Sci. Lett., 23,* 265–274, 1974*b*.

Quaide, W. L., D. E. Gault, and R. A. Schmidt, Gravitation effects on lunar impact structures, *Ann. N. Y. Acad. Sci., 123,* 563–572, 1965.

Rumsey, H. C., G. A. Morris, R. R. Green, and R. M. Goldstein, A radar brightness and altitude image of a portion of Venus, *Icarus, 23,* 1–7, 1974.

Schultz, P. H., and D. E. Gault, Seismic effects from major basin formation, *Moon, 12,* 159–177, 1975.

Shoemaker, E. M., Interpretation of lunar craters, in *Physics and Astronomy of the Moon,* edited by Z. Kopal, pp. 283–359, Academic, New York, 1962.

Shoemaker, E. M., Impact mechanics at Meteor Crater, Arizona, in *The Solar System,* vol. 4, edited by G. Kuiper, pp. 301–336, University of Chicago Press, Chicago, Ill., 1963.

Smith, E. I., and A. G. Sanchez, Fresh lunar craters: Morphology as a function of diameter, a possible criterion for crater origin, *Mod. Geol., 4,* 51–59, 1973.

Stöffler, D., D. E. Gault, J. Wedekind, and G. Polkowski, Experimental hypervelocity impact into quartz sand: Distribution and shock metamorphism of ejecta, *J. Geophys. Res., 80,* in press, 1975.

Stuart-Alexander, D. E., and K. A. Howard, Lunar maria and circular basins—A review, *Icarus, 12*(3), 440–456, 1970.

Trask, N. J., and J. E. Guest, Preliminary geologic terrain map of Mercury, *J. Geophys. Res., 80,* this issue, 1975.

Varnes, D.J., Landslide types and processes, Landslides and Engineering Practice, *Publ. 544,* pp. 20–47, Nat. Acad. of Sci., Washington, D. C., 1958.

Viktorov, V. V., and R. D. Stepenov, Modeling of the action of an explosive with concentrated charges in uniform (homogeneous) ground, *Inzh. Sb., 28,* 87–96, 1960. (English translation, Sandia Corporation, Albuquerque, N. Mex.)

Wetherill, G. W., Pre-mare cratering and early solar system history, in *Proceedings of the Soviet-American Conference on Cosmochemistry of the Moon and Planets,* NASA, Washington, D. C., in press, 1975.

Wood, C. A., Moon: Central peak heights and crater origins, *Icarus, 20,* 503–506, 1973.

(Received February 7, 1975;
revised March 3, 1975;
accepted March 3, 1975.)